Electron thermal confinement in a partially stochastic magnetic structure

L. A. Morton, W. C. Young, C. C. Hegna, E. Parke, J. A. Reusch, and D. J. Den Hartog

Citation: Physics of Plasmas **25**, 042306 (2018); doi: 10.1063/1.5021893
View online: https://doi.org/10.1063/1.5021893
View Table of Contents: http://aip.scitation.org/toc/php/25/4
Published by the American Institute of Physics

Electron thermal confinement in a partially stochastic magnetic structure

L. A. Morton,[1,a)] W. C. Young,[1] C. C. Hegna,[2] E. Parke,[3] J. A. Reusch,[2] and D. J. Den Hartog[1]

[1]*Department of Physics, University of Wisconsin-Madison, 1150 University Avenue, Madison, Wisconsin 53706, USA*

[2]*Department of Engineering Physics, University of Wisconsin-Madison, 1500 Engineering Drive, Madison, Wisconsin 53706, USA*

[3]*Department of Physics and Astronomy, University of California Los Angeles, 475 Portola Plaza, Los Angeles, California 90095, USA*

(Received 9 January 2018; accepted 26 March 2018; published online 13 April 2018)

Using a high-repetition-rate Thomson scattering diagnostic, we observe a peak in electron temperature T_e coinciding with the location of a large magnetic island in the Madison Symmetric Torus. Magnetohydrodynamic modeling of this quasi-single helicity plasma indicates that smaller adjacent islands overlap with and destroy the large island flux surfaces. The estimated stochastic electron thermal conductivity ($\approx 30\,m^2/s$) is consistent with the conductivity inferred from the observed T_e gradient and ohmic heating power. Island-shaped T_e peaks can result from partially stochastic magnetic islands. *Published by AIP Publishing*. https://doi.org/10.1063/1.5021893

I. INTRODUCTION

The transport of particles along stochastic trajectories is an important phenomenon in both plasma[1] and fluid turbulence.[2] Stochastic transport may play a role in tokamak and stellarator divertor control,[3] avoidance of edge instabilities in tokamaks,[4] and core confinement improvement in the spherical tokamak[5] and reversed-field pinch (RFP).[6] In the following, we report a quantitative comparison between theoretical modeling and experimental observations of plasma transport processes in a partially stochastic magnetic structure (that is, one in which the stochastic transport approaches the level of transport across closed flux surfaces).

The RFP presents a test case for electron thermal transport in magnetic stochasticity. A standard RFP plasma contains many tearing mode magnetic islands that form at the magnetic flux surfaces where the safety factor q (a measure of the field line pitch) takes on low-order rational values.[7] Overlap of islands with different helicities produces stochastic magnetic field lines. The dominant radial transport mechanism in the RFP core is rapid parallel transport along highly stochastic magnetic field lines.[8,9]

The degree of stochasticity and transport varies cyclically during the quasi-periodic sawtooth cycle. In the standard RFP, the parallel current density tends to peak on-axis due to the balance between inductive drive and ohmic dissipation.[6,10] The gradual ramp-up of the parallel current density ends with a sawtooth crash. During the crash, tearing mode instabilities (which exist at moderate amplitudes during the ramp phase) rapidly grow to large amplitude, resulting in increased stochasticity and reduced confinement.[8] The nonlinear interaction of the modes also acts to flatten the parallel current profile, restarting the cycle.[10] At high plasma current, the core-most tearing mode tends to grow larger between sawteeth, while the others decay, resulting in a quasi-single helicity (QSH) state: a coherent helical magnetic structure with locally improved confinement.[11,12]

Hot island-shaped structures are observed in the RFX-mod RFP during QSH,[11–14] with local electron thermal conductivity $\chi_e \approx 10\,m^2/s$,[15] much lower than the typical values of several hundred meters squared per second in the stochastic region. These hot structures were associated with remnant islands, which are closed nested flux surfaces remaining around the O-points of magnetic islands, surrounded by stochastic magnetic field lines. The Madison Symmetric Torus (MST) and the EXTRAP T2R RFPs have also produced signatures of locally improved confinement within remnant islands.[16,17] However, locally improved confinement might occur even without the restoration of closed helical flux surfaces within an island, as long as the magnetic field line diffusion rate is sufficiently reduced. Recent theoretical results suggest that transport barriers may be hidden within stochastic fields.[18] In tokamaks, isolated magnetic islands often exist with good helical flux surfaces, but ohmic heating is not observed to cause hot islands.[19–22] However, there is a recent experimental evidence that electrostatic turbulent transport is reduced inside large islands.[23,24]

In Sec. II, we report agreement between the observed conductivity $\chi_e \approx 27 \pm 5\,m^2/s$ within a stochastic, an island-shaped electron temperature (T_e) structure in the Madison Symmetric Torus (MST) RFP, and the estimated conductivity $\chi_e \approx 30\,m^2/s$ due to stochastic transport in that region. The stochastic structure results from the destruction of a large magnetic island with poloidal and toroidal mode numbers $m = 1, n = 6$ by overlap with smaller neighboring islands. A two-dimensional view of the T_e structure is captured in a single discharge for the first time in an RFP by the new high-repetition-rate Thomson scattering (TS) laser.[25–27] We demonstrate that peaked island-shaped T_e structures do not necessarily imply remnant islands in which closed flux surfaces fill the majority of the island volume.

In Sec. III, we provide an evidence for heating of $n = 6$ magnetic structures using statistical analysis of a large dataset

a)Present address: Department of Engineering Physics, University of Wisconsin-Madison, 1500 Engineering Drive, Madison, Wisconsin 53706, USA. Electronic mail: lamorton@wisc.edu.

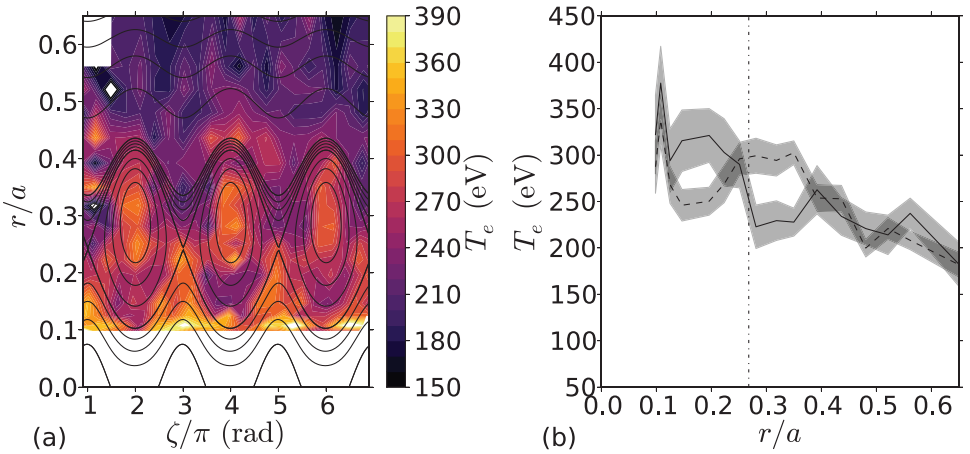

FIG. 1. (a) T_e as a function of normalized minor radius r/a and $n = 6$ magnetic mode phase ζ. Radius and phase have been corrected for the Shafranov shift. The black curves are contours of $n = 6$ helical magnetic flux. (b) T_e at time points where the X and O points of the island (solid and dashed lines, respectively) are near the TS diagnostic. The shading indicates standard deviation uncertainty. The vertical line marks the rational surface radius.

of fluctuation measurements at lower TS sampling rate. In particular, the strong radial asymmetry of the second and higher harmonics of the T_e fluctuation correlated to the magnetic mode phase is inconsistent with an isothermal model for a magnetic island, even when the possibility of asymmetry of the underlying magnetic island is considered. These measurements show that the phenomenon of heating in (possibly stochastic) islands occurs more generally during the sawtooth cycle on MST, not only during QSH periods.

II. SINGLE-SHOT RESULTS WITH HIGH-REPETITION-RATE THOMSON LASER

MST discharge 1140726089 displays clear T_e fluctuations correlated with the $n = 6$ tearing mode, shown in Fig. 1. Firing 25 pulses at 66 kHz repetition rate, the new Thomson scattering (TS) laser provided several radial profiles through the structure per period as it rotated toroidally past the diagnostic at 10 kHz. The hot spots near normalized minor radius $r/a \approx 0.3$ (where the minor radius of MST is $a = 52$ cm) coincide with the O-point of a 16-cm wide island in the $n = 6$ helical flux, as determined by MHD modeling (described below). The helical flux surfaces in Fig. 1(a) have not been adjusted to fit the T_e structure, being derived from modeling based only on edge magnetic measurements. The core region between the island and the magnetic axis (at $r/a = 0$) is also heat-confining, probably due to the presence of unbroken flux surfaces as indicated by field line tracing described below.

The discharge parameters are plasma current $I_p \approx 400$ kA, line-averaged electron density $n_e \approx 1.6 \times 10^{19}$ m^{-3}, and reversal parameter of the toroidal field $F \equiv B_\phi(a)/\langle B_\phi \rangle \approx -0.3$. The edge amplitude $B_\theta^{(1,6)}(a)$ of the $n = 6$ mode is 13 G at this time, or 0.9% of the mean poloidal field at the wall. The $n = 5$ amplitude is 0.75 G, and the $n \geq 7$ amplitudes are 2.5 G or less. This constitutes a QSH state.

A. MHD modeling

The magnetic fields used to compute the $n = 6$ helical flux in Fig. 1(a) were found as follows. MSTFIT, an axisymmetric Grad-Shafranov equilibrium solver,[28] reconstructed the mean magnetic fields. The B_θ and q profiles from MSTFIT were used with the relation $q = rB_\phi/R_0B_\theta$ to find the correct B_ϕ to use in the periodic cylindrical geometry adopted for the rest of the calculations in this work. ($R_0 = 1.5$ m is the major radius of MST.) The tearing mode magnetic perturbations were derived from DEBS[29] nonlinear single-fluid visco-resistive MHD simulations in periodic cylindrical geometry detailed in Ref. 8, using the following methodology. The profiles of $\mathbf{B}^{(m,n)}(r)$ for each mode were averaged over times where the reversal parameter was close to the experimental value during the sawtooth cycle of these initial-value simulations. The $n = 6$ profile is consistent with the results from the previous experiments using a polarimetry diagnostic.[30] Each mode profile was scaled to have the same $B_\theta^{(m,n)}(r = a)$ as measured in MST at the measurement time. (DEBS simulations typically yield saturated mode amplitudes twice as large as those measured in MST.[8,9]) Figure 2 summarizes the resulting island widths and resonant locations, where $q(r) = -m/n$.

B. Magnetic stochasticity

The flux surfaces of Fig. 1(a) exist only in the single-helicity approximation. As shown in Fig. 2, the $n = 7$ and $n = 8$ islands overlap the $n = 6$ island. The MAL code[8,9] was used to trace field lines using a magnetic field incorporating the $n = 5$ through $n = 10$ modes, scaled as described above. Figure 3 shows that despite the island overlap and resulting stochasticity, field lines still follow the $n = 6$ island surfaces

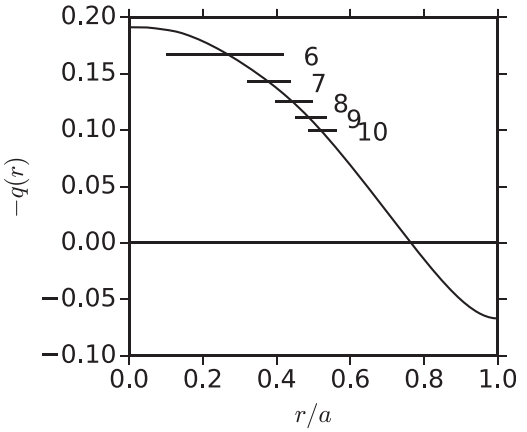

FIG. 2. Safety factor profile from MSTFIT. Horizontal bars indicate the resonant location and width of tearing mode islands, labeled by toroidal mode number, with poloidal mode number $m = 1$.

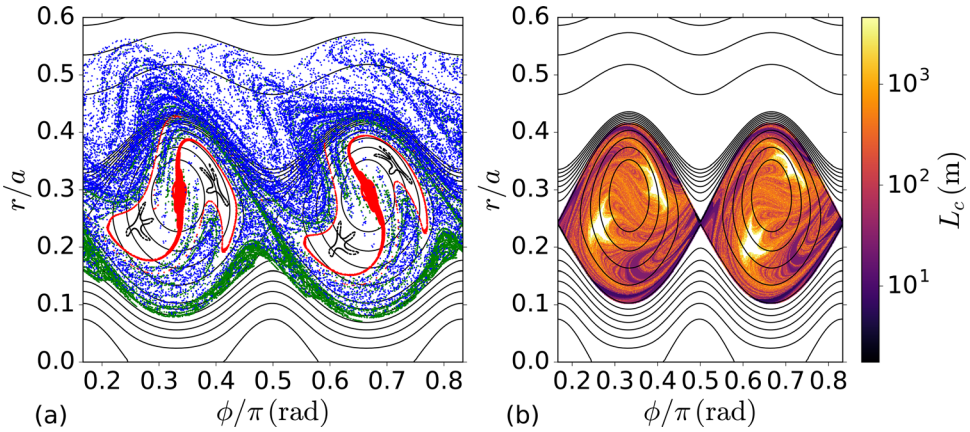

FIG. 3. (a) Poincaré plot of the stochastic field at poloidal angle $\theta = 0$. Black contours are $n = 6$ flux surfaces. Red field lines were launched near the O-point, blue lines at the high-r side of the separatrix, and green lines from the low-r side (the core). Lines were traced for $\lambda_{mfp} \approx 125$ m. The black field line lies on a remnant flux surface. It was traced ≈1 km. (b) Connection length to the separatrix.

to a degree, especially near the separatrix. Thus, the observed T_e structure could reflect the $n = 6$ island shape.

There are several features of note in the stochastic field in Fig. 3. The pattern of lobes is reminiscent of a homoclinic tangle, such as is illustrated by Evans *et al.*[31] Small remnants exist of a secondary island, formed where the $n = 7$ perturbation is resonant with the field line pitch of the unperturbed $n = 6$ island. Some of the complex field line structure may be reflected in Fig. 1(a), although a firm conclusion is not possible given the diagnostic uncertainty during this discharge. The core region (near $r = 0$) contains closed surfaces, which matches the hot core seen in Fig. 1(a). Varying the mode amplitudes by up to 20% (within uncertainties) can lead to remnant island flux surfaces surrounding the O-point, or to somewhat larger remnant secondary islands. While we cannot rule out these scenarios, the present analysis is focused on the most probable configuration according to our modeling.

We define the connection length L_c within the stochastic field region inside the (single-helicity) separatrix as the distance along a field line at which the field line first escapes through the separatrix. Figure 3(b) demonstrates that a large fraction of the field lines inside the separatrix have $L_c > \lambda_{mfp}$, where $\lambda_{mfp} \approx 125$ m is the electron collisional mean free path. Thus, thermal isolation of the island interior is plausible. L_c grows exponentially approaching the remnant secondary islands.

C. Stochastic transport estimate

We estimate the thermal transport along the stochastic magnetic field using a diffusive random walk approximation. We take the time step of the random walk to be the electron-ion collision time $\tau_{ei} \approx 1.1 \times 10^{-5}$ s. During a collision time, an electron moving with thermal velocity $v_{th,e} \approx 1.1 \times 10^7$ m/s will travel one mean free path length $\lambda_{mfp} \approx 125$ m. Therefore, we evaluate the dispersal $\delta^2 \equiv \langle(\Delta\rho)^2\rangle$ for 1000 lines launched from near the O-point and followed for a distance of 125 m. Here, $\Delta\rho = \rho(L) - \rho(0)$ is the displacement of a field line in terms of ρ, the distance radially outward from the O-point to the flux surface. Evaluating δ^2 at $L = 125$ m yields $\delta^2 = 1.1 \times 10^{-3}$ m^2.

Figure 4(a) shows the behavior of δ^2 over field line length L. For intermediate values of L, $\delta^2 \propto L^3$, indicating super-diffusive[32] field line motion. (Diffusion is characterized by $\delta^2 \propto L$.) Super-diffusion indicates correlated field line trajectories. The dispersal saturates for $L > 200$ m as the field line distribution equilibrates in the finite stochastic volume.

Mirror trapping reduces the thermal conductivity along field lines as shown in Ref. 8. This effect is quantified by the effective passing fraction f_p. To estimate the total reduction of parallel heat flux from trapped particle effects including trapped-passing collisions (but considering only the axisymmetric field), we refer to Ref. 33. At the rational surface

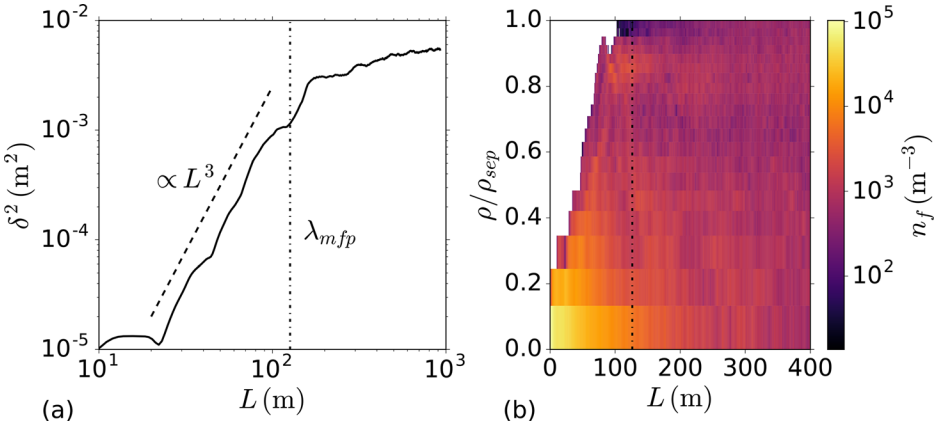

FIG. 4. (a) Field line dispersal as a function of field line length. (b) Number density of field lines as a function of island effective radius.

radius, the inverse aspect ratio is $\epsilon \approx 0.1$. We estimate that the ratio of parallel temperature gradient length L_T to the collision length λ_{mfp} is between 10^0 and 10^2. From Fig. 4 in Ref. 33, an estimate for the parallel heat flux fractional reduction is $f_t = 1 - f_p \approx 0.4$ for these conditions.

The form of our stochastic diffusion estimate is thus[8]

$$\chi_{e,m} = f_p \frac{\delta^2}{2\tau_{ei}}. \tag{1}$$

Combining the values for these quantities estimated above, we arrive at $\chi_{e,m} \approx 30\,\mathrm{m}^2/\mathrm{s}$.

D. Power balance transport estimate

To compare with this stochastic transport estimate, we calculate the thermal transport by assuming that the electron number density n_e, ohmic heating power density ηJ^2, and effective perpendicular thermal conductivity χ_e are spatially constant and that the temperature is constant in time. Integration of the thermal energy continuity equation

$$-\nabla \cdot \boldsymbol{Q} + \eta J^2 = 0, \tag{2}$$

with a conductive model for the heat transport

$$\boldsymbol{Q} = -n_e \chi_e \nabla T_e, \tag{3}$$

over the volume enclosed by a flux surface yields

$$\eta J^2 = n_e\, \chi_e \left\langle \nabla T_e \right\rangle \left(\frac{A}{V}\right), \tag{4}$$

where A is the area of a flux surface, V is the enclosed volume inside the surface, Ψ is the $n = 6$ helical flux, and

$$\left\langle \nabla T_e \right\rangle \equiv -\frac{\partial T_e}{\partial \Psi} \left(\frac{1}{A} \oint \nabla \Psi \cdot d\boldsymbol{A}\right) \tag{5}$$

is the average temperature gradient over the flux surface. Eliminating $\langle \nabla T_e \rangle$ from Eqs. (4) and (5) while solving for the temperature gradient in terms of flux yields

$$\frac{\partial T_e}{\partial \Psi} = -\left(\frac{\eta J^2}{n_e\, \chi_e}\right) \left(\frac{V}{\oint \nabla \Psi \cdot d\boldsymbol{A}}\right), \tag{6}$$

where, under our assumptions, the first factor on the right-hand side is constant with respect to flux (except for step changes in χ_e across the separatrix). Integrating Eq. (6) with respect to flux yields

$$T_e(\Psi) = -\left(\frac{\eta J^2}{n_e\, \chi_e}\right) \int \frac{V}{\oint \nabla \Psi \cdot d\boldsymbol{A}} d\Psi + const. \tag{7}$$

Thus, once the geometric integral has been performed and the particle and power densities have been fixed, the temperature as a function of flux becomes a linear model with two parameters (the boundary temperature and the inverse conductivity). In order to model all three topological regions of the plasma (island, core, and exterior), we allow a different conductivity for each region, which is spatially constant within a given region. The separatrix temperature is used as the boundary condition for all three regions. Thus, the overall model consists of three conductivities plus the separatrix temperature. We performed a least-squares optimization (weighted by the measurement uncertainties) to find the best-fit value of these four parameters such that our model best reproduced the measured temperature values.

This model results in an estimate of $\chi_e \approx 27 \pm 5\,\mathrm{m}^2/\mathrm{s}$ for the island, at the 95% confidence level, incorporating only the statistical uncertainties from the measurements of T_e. Figure 5 shows the results of the fitting process in terms of the electron temperature as a function of helical flux. (The T_e dataset was restricted to select measurement points with relative uncertainties <25%.) The ohmic heating power density (estimated in MSTFIT via the Spitzer resistivity with $Z_{eff} \approx 2$) is $\eta J^2 \approx 1.3 \times 10^6\,\mathrm{W/m}^3$, and the electron density is $n_e \approx 1.6 \times 10^{19}\,\mathrm{m}^{-3}$. The uncertainties in these quantities have not been quantified and propagated to the conductivity.

There is some visual indication in Fig. 1 that the confinement is occurring primarily near the O-point rather than uniformly across the island radius, in which case a non-constant conductivity model might be more appropriate. This would be expected as well from the field line tracing, which shows that the field line diffusion is more rapid at the periphery of the island. The present estimates (both for the power balance and the stochastic conductivities) should be understood as effective values for the whole structure.

We obtained several other observations of T_e peaking, with lower signal-to-noise ratio. Field line tracing indicates remnant islands in these cases. In some instance, no T_e structure is observed despite the prediction of a remnant island. This is consistent with the previous research indicating that thermal confinement during QSH is intermittent, in ways not explained by trends in the secondary mode amplitudes as measured at the plasma edge.[14,34] The observation detailed in

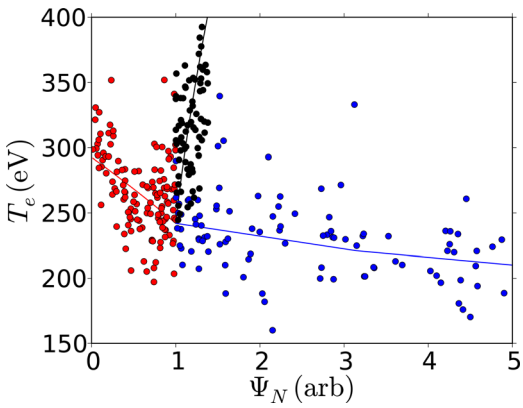

FIG. 5. Electron temperature as mapped to normalized helical flux Ψ_N, which is zero at the island O-point and 1 at the separatrix. Red: within the island; black: core region (between inner side of separatrix and the magnetic axis); blue: exterior (between outer side of the separatrix and the wall). Because Ψ_N is non-monotonic in radius, the core and the exterior appear as separate branches. The solid lines represent the least-squares fit model with conductivities of 27, 5.4, and 150 m^2/s for the island, core, and exterior, respectively, and the separatrix temperature 242 eV.

this work occurred during the growth phase of the QSH state, which is more likely to exhibit strong thermal confinement.[14]

D. Discussion

As shown in Fig. 5, the core region (between the inner side of the separatrix and the magnetic axis) and the exterior region (between the outer side of the separatrix and the wall) have power-balance conductivities of about 5 and 150 m^2/s, respectively. The conductivity of the partially stochastic region is mid-way between these extremes at $\approx 30\,m^2/s$. Thus, stochastic transport appears to be reduced but not eliminated in this structure.

The thermal confinement in the partially stochastic magnetic structure is close to values reported previously for helical structures in RFX-mod and MST. In RFX-Mod, Annibaldi *et al.* derive a power-balance thermal conductivity as low as $10\,m^2/s$ for island-shaped electron temperature hot structures.[15] Previous power-balance studies of thermal confinement in $n = 5$ magnetic structures in MST also yielded $\approx 30\,m^2/s$ minimum electron conductivity, using only ensemble-averaged measurements.[35]

The power-balance estimate of the conductivity in the exterior region is consistent with the previous estimates made for MST. In Ref. 8, the stochastic transport estimate and power balance estimates for the range of 1–2 ms following a sawtooth crash are about $\approx 100-200\,m^2/s$, which agrees well with the power-balance estimate found in this work ($\approx 150\,m^2/s$). The conductivity in the exterior, fully stochastic region is several times higher than our estimate for the conductivity in the partially stochastic magnetic structure.

III. ENSEMBLE MEASUREMENTS AND ANALYSIS

A large collection of Thomson scattering data is available using the 25 kHz Thomson scattering laser.[36] The system comprises two lasers whose individual bursts have up to 4 pulses at 80 μs. The two lasers can be interleaved to achieve bursts of up to 8 pulses at 40 μs period. Alternately, the relative starting times of the two lasers can be adjusted independently to produce bursts of pulse pairs, with each pair having a time delay as small as 1 μs. In this dataset, the lasers were fired with a range of spacing between 1 and 5 μs.

We analyze this data to understand the interaction of the $n = 5$ and $n = 6$ modes at more representative amplitudes for standard discharges. These bursts were acquired during the interval of one to three milliseconds following a sawtooth crash by using a real-time sawtooth detector circuit to trigger the 25 kHz TS laser. About 600 bursts were available for which $I_p \approx 400$ kA, $n_e = 0.8$ to $1.2 \times 10^{19}\,m^{-3}$, and the plasma rotation was not locked to the wall. Due to data quality, about 400 to 500 bursts were used for each radial point in the core, whereas the two edge-most points had only about 200 bursts. (Acceptable bursts are defined by having <30% T_e uncertainty for each measurement in the burst.)

Correlating the temperature fluctuations to the magnetic mode phase over a large ensemble using the model $T_e(r,t) = T_{e,0}(r) + \tilde{T}_e(r)\cos(\phi_{m,n} + \delta_{m,n})$ yields the mode-induced temperature fluctuations, despite the short burst length (8 laser pulses) and a Nyquist frequency that is comparable to the mode frequency.[35,37] In this work, the higher harmonics of the form $\tilde{T}_e(r)\cos(\nu\phi_{m,n} + \delta_{\nu,m,n})$, with harmonic number $\nu > 1$, were also considered. (The phase of the higher harmonics was allowed to vary in the fit, so that the relative phase between the fundamental and higher harmonics was not assumed from the outset but was rather found from the data.)

The temperature fluctuation profiles of the $n = 5$ to 7 fluctuations in Fig. 6(a) illustrate that the mode-induced temperature fluctuations overlap significantly. This suggests that the magnetic field may be stochastic. Despite the probable absence of closed flux surfaces, the temperature fluctuations stand out very clearly, demonstrating that each mode is able to modify transport in the region where it is closest to resonance. The $n = 6$ fundamental exhibits the characteristic[38] zero-crossing in amplitude (and reversal in phase, not shown) at the rational surface location $r/a \approx 0.3$, as expected for a tearing-type mode. While the signal-to-noise ratio is lower, the $n = 7$ mode also appears to have tearing-type characteristics. The $n = 5$ mode is either non-resonant or its resonant surface may be very close to the magnetic axis.

The higher harmonics ($\nu = 2, 3$) of the $n = 6$ fluctuations have significant amplitude in this ensemble [see Fig. 6(b)]. The strong, highly asymmetric higher harmonics contrast with the relatively small, symmetric higher-harmonic content for the isothermal island model,[38] suggesting that there is heating even in non-QSH conditions. The fact that the higher harmonics do not go to zero at the same location as the fundamental ($\nu = 1$) demonstrates variation of the temperature inside the island volume, since there is no radius at which all harmonics are simultaneously zero, as would be expected for an isothermal island.

This logic even holds when we allow for the possibility of asymmetry in the underlying magnetic island structure, as

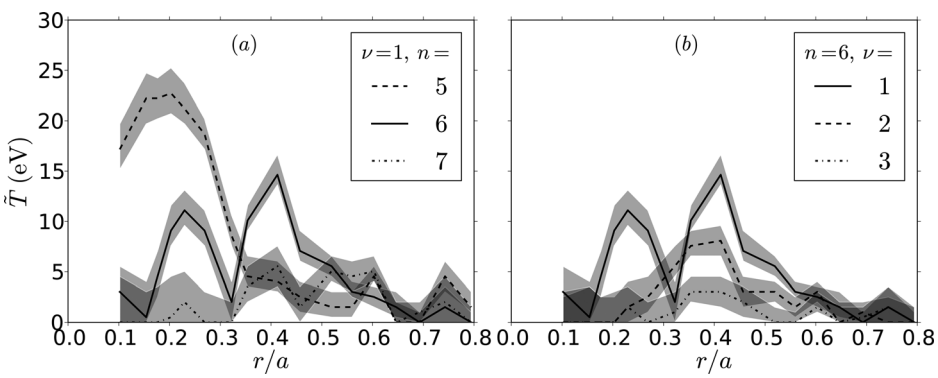

FIG. 6. (a) Radial profiles of the electron temperature fluctuation amplitude correlated with the $n = 5$ to 7 magnetic modes. (b) Radial profiles of the first three harmonics of electron temperature fluctuation correlated with the $n = 6$ magnetic mode.

seen in the fluctuations produced by asymmetric island models.[20,23] Island helical flux surface asymmetry is evident in the flux surfaces of the $n = 6$ island in Sec. II, in that the X-point is shifted radially inward with respect to the O-point. This displacement is due to the finite first derivative of the $n = 6$ mode's perturbed helical flux profile. In an isothermal model of such an asymmetric island, fluctuations of all orders still go to zero at the radius of the X-points, which is in contradiction with our observations. However, both island heating and island asymmetry can displace the zero-crossing of the fundamental away from the rational surface radius. This could necessitate small corrections to the resonant surface location for efforts (such as those of Parke *et al.*[37]) to constrain the safety factor profile based on T_e fluctuation profiles, especially if only the fundamental is considered.

The profiles of both the relative amplitudes and phases of the ensemble fluctuations shown in Fig. 6 are similar to the fluctuation results obtained when applying the same correlation analysis to the observed hot island-like structure in Sec. II, which shows that the ensemble results are consistent with this origin. The overall amplitude of the ensemble-averaged fluctuations is smaller by a factor of about three, which is consistent with the fact that the conditions in Sec. II were more favorable than those of the ensemble for the production of a large region of reduced stochasticity. Nevertheless, these results suggest that enhanced local confinement associated with the $n = 6$ magnetic mode is relatively common between sawteeth in standard MST discharges, not only in QSH situations.

IV. CONCLUSION

In conclusion, we have shown that temperature peaking can occur even inside island-shaped partially stochastic structures, not only in remnant islands (those whose interior is filled predominantly with good flux surfaces). The shape and the confinement properties of the observed T_e structure are consistent with our magnetic field modeling and diffusive transport approximation, respectively, supporting this conclusion. We thus demonstrate that the observation of hot-island-like temperature structures does not necessarily indicate the presence of a remnant island in RFP discharges, since appreciable temperature gradients can be supported in partially stochastic magnetic fields. Appropriate field-line tracing and plotting techniques help to identify such structures in modeled magnetic fields, which could otherwise go undetected.

Future research is warranted to compare numerical transport simulations (for instance, fluid calculations as in Ref. 39 or non-local closures as in Refs. 33 and 40) to the diffusive approximation applied in this work, and to experimental observations, in complex magnetic fields structures of this type.

SUPPLEMENTARY MATERIAL

See supplementary material for data shown in all figures.

ACKNOWLEDGMENTS

This material was based upon the work supported by the U.S. Department of Energy, Office of Science, Office of Fusion Energy Sciences under Award No. DE-FC02–05ER54814 and by the National Science Foundation under Award No. PHY-0821899, as well as the General Atomics Postgraduate Research Participation Program administered by ORAU. We acknowledge helpful discussions with J. D. Callen, C. M. Jacobson, L. M. Reusch, J. S. Sarff, and H. D. Stephens.

[1]O. Schmitz, Nucl. Fusion **52**, 54001 (2012).
[2]G. Haller, Annu. Rev. Fluid Mech. **47**, 137 (2015).
[3]R. König, P. Grigull, K. McCormick, Y. Feng, J. Kisslinger, A. Komori, S. Masuzaki, K. Matsuoka, T. Obiki, N. Ohyabu, H. Renner, F. Sardei, F. Wagner, and A. Werner, Plasma Phys. Controlled Fusion **44**, 2365 (2002).
[4]T. E. Evans, R. A. Moyer, P. R. Thomas, J. G. Watkins, T. H. Osborne, J. A. Boedo, E. J. Doyle, M. E. Fenstermacher, K. H. Finken, R. J. Groebner, M. Groth, J. H. Harris, R. J. La Haye, C. J. Lasnier, S. Masuzaki, N. Ohyabu, D. G. Pretty, T. L. Rhodes, H. Reimerdes, D. L. Rudakov, M. J. Schaffer, G. Wang, and L. Zeng, Phys. Rev. Lett. **92**, 235003 (2004).
[5]K. L. Wong, S. M. Kaye, D. R. Mikkelsen, J. A. Krommes, K. Hill, R. Bell, and B. LeBlanc, Phys. Plasmas **15**, 056108 (2008).
[6]J. K. Anderson, J. Adney, A. Almagri, A. Blair, D. L. Brower, M. Cengher, B. E. Chapman, S. Choi, D. Craig, D. R. Demers, D. J. Den Hartog, B. H. Deng, W. X. Ding, F. Ebrahimi, D. Ennis, G. Fiksel, C. B. Forest, P. Franz, J. Goetz, R. W. Harvey, D. Holly, B. Hudson, M. Kaufman, T. Lovell, L. Marrelli, P. Martin, K. McCollam, V. V. Mirnov, P. Nonn, R. O'Connell, S. Oliva, P. Piovesan, S. C. Prager, I. Predebon, J. S. Sarff, G. Spizzo, V. Svidzinski, M. Thomas, and M. D. Wyman, Phys. Plasmas **12**, 056118 (2005).
[7]S. Ortolani and D. D. Schnack, *Magnetohydrodynamics of Plasma Relaxation* (World Scientific, Singapore, 1993).
[8]J. A. Reusch, J. K. Anderson, D. J. Den Hartog, F. Ebrahimi, D. D. Schnack, H. D. Stephens, and C. B. Forest, Phys. Rev. Lett. **107**, 155002 (2011).
[9]T. M. Biewer, C. B. Forest, J. K. Anderson, G. Fiksel, B. Hudson, S. C. Prager, J. S. Sarff, J. C. Wright, D. L. Brower, W. X. Ding, and S. D. Terry, Phys. Rev. Lett. **91**, 045004 (2003).
[10]B. H. Deng, W. X. Ding, D. L. Brower, A. F. Almagri, K. J. McCollam, Y. Ren, S. C. Prager, J. S. Sarff, J. A. Reusch, and J. K. Anderson, Plasma Phys. Controlled Fusion **50**, 115013 (2008).
[11]P. Martin, L. Marrelli, A. Alfier, F. Bonomo, D. F. Escande, P. Franz, L. Frassinetti, M. Gobbin, R. Pasqualotto, P. Piovesan, D. Terranova, and RFX-mod Team, Plasma Phys. Controlled Fusion **49**, A177 (2007).
[12]D. F. Escande, P. Martin, S. Ortolani, A. Buffa, P. Franz, L. Marrelli, E. Martines, G. Spizzo, S. Cappello, A. Murari, R. Pasqualotto, and P. Zanca, Phys. Rev. Lett. **85**, 1662 (2000).
[13]L. Carraro, A. Alfier, F. Bonomo, A. Fassina, M. Gobbin, R. Lorenzini, P. Piovesan, M. E. Puiatti, G. Spizzo, D. Terranova, M. Valisa, M. Zuin, A. Canton, P. Franz, P. Innocente, R. Pasqualotto, F. Auriemma, S. Cappello, S. C. Guo, L. Marrelli, E. Martines, M. Spolaore, and L. Zanotto, Nucl. Fusion **49**, 55009 (2009).
[14]P. Franz, M. Gobbin, L. Marrelli, A. Ruzzon, F. Bonomo, A. Fassina, E. Martines, and G. Spizzo, Nucl. Fusion **53**, 53011 (2013).
[15]S. V. Annibaldi, F. Bonomo, R. Pasqualotto, G. Spizzo, A. Alfier, P. Buratti, P. Piovesan, and D. Terranova, Phys. Plasmas **14**, 112515 (2007).
[16]P. Franz, L. Marrelli, P. Piovesan, I. Predebon, F. Bonomo, L. Frassinetti, P. Martin, G. Spizzo, B. E. Chapman, D. Craig, and J. S. Sarff, Phys. Plasmas **13**, 012510 (2006).
[17]L. Frassinetti, P. R. Brunsell, J. R. Drake, S. Menmuir, and M. Cecconello, Phys. Plasmas **14**, 112510 (2007).
[18]G. Rubino, D. Borgogno, M. Veranda, D. Bonfiglio, S. Cappello, and D. Grasso, Plasma Phys. Controlled Fusion **57**, 85004 (2015).
[19]J. A. Snape, K. J. Gibson, T. O'Gorman, N. C. Barratt, K. Imada, H. R. Wilson, G. J. Tallents, I. T. Chapman, and MAST Team, Plasma Phys. Controlled Fusion **54**, 85001 (2012).
[20]J. P. Meskat, H. Zohm, G. Gantenbein, S. Günter, M. Maraschek, W. Suttrop, Q. Yu, and ASDEX Upgrade Team, Plasma Phys. Controlled Fusion **43**, 1325 (2001).
[21]I. G. J. Classen, E. Westerhof, C. W. Domier, A. J. H. Donné, R. J. E. Jaspers, N. C. Luhmann, Jr., H. K. Park, M. J. van de Pol, G. W. Spakman, and M. W. Jakubowski, Phys. Rev. Lett. **98**, 035001 (2007).
[22]H. J. van der Meiden, S. K. Varshney, C. J. Barth, T. Oyevaar, R. Jaspers, A. J. H. Donné, M. Y. Kantor, D. V. Kouprienko, E. Uzgel, W. Biel, A. Pospieszczyk, and TEXTOR Team, Rev. Sci. Instrum. **77**, 10E512 (2006).

[23]L. Bardóczi, T. L. Rhodes, T. A. Carter, N. A. Crocker, W. A. Peebles, and B. A. Grierson, Phys. Plasmas **23**, 052507 (2016).
[24]L. Bardóczi, T. L. Rhodes, T. A. Carter, A. Bañón Navarro, W. A. Peebles, F. Jenko, and G. McKee, Phys. Rev. Lett. **116**, 215001 (2016).
[25]W. C. Young and D. J. Den Hartog, J. Instrum. **10**, C12021 (2015).
[26]W. C. Young, L. A. Morton, E. Parke, and D. J. Den Hartog, J. Instrum. **8**, C11013 (2013).
[27]W. S. Harris, D. J. Den Hartog, and N. C. Hurst, Rev. Sci. Instrum. **81**, 10D505 (2010).
[28]J. K. Anderson, C. B. Forest, T. M. Biewer, J. S. Sarff, and J. C. Wright, Nucl. Fusion **44**, 162 (2004).
[29]D. D. Schnack, D. C. Barnes, Z. Mikic, D. S. Harned, and E. J. Caramana, J. Comput. Phys. **70**, 330 (1987).
[30]L. Lin, W. X. Ding, and D. L. Brower, Rev. Sci. Instrum. **85**, 11D403 (2014).
[31]T. E. Evans, R. K. W. Roeder, J. A. Carter, B. I. Rapoport, M. E. Fenstermacher, and C. J. Lasnier, J. Phys.: Conf. Ser. **7**, 174 (2005).
[32]D. Perrone, R. O. Dendy, I. Furno, R. Sanchez, G. Zimbardo, A. Bovet, A. Fasoli, K. Gustafson, S. Perri, P. Ricci, and F. Valentini, Space Sci. Rev. **178**, 233 (2013).
[33]E. D. Held, J. D. Callen, and C. C. Hegna, Phys. Plasmas **10**, 3933 (2003).
[34]S. Munaretto, B. E. Chapman, M. D. Nornberg, J. Boguski, A. M. DuBois, A. F. Almagri, and J. S. Sarff, Phys. Plasmas **23**, 056104 (2016).
[35]H. D. Stephens, D. J. Den Hartog, C. C. Hegna, and J. A. Reusch, Phys. Plasmas **17**, 056115 (2010).
[36]D. J. Den Hartog, J. R. Ambuel, M. T. Borchardt, A. F. Falkowski, W. S. Harris, D. J. Holly, E. Parke, J. A. Reusch, P. E. Robl, H. D. Stephens, and Y. M. Yang, Rev. Sci. Instrum. **81**, 10D513 (2010).
[37]E. Parke, J. K. Anderson, D. L. Brower, D. J. Den Hartog, W. X. Ding, C. A. Johnson, and L. Lin, Phys. Plasmas **23**, 056108 (2016).
[38]R. Fitzpatrick, Phys. Plasmas **2**, 825 (1995).
[39]S. R. Hudson and J. Breslau, Phys. Rev. Lett. **100**, 095001 (2008).
[40]D. Del-Castillo-Negrete and L. Chacón, Phys. Plasmas **19**, 056112 (2012).